ACS OMEGA

Open Access

This article is licensed under CC-BY-NC-ND 4.0

http://pubs.acs.org/journal/acsodf

Article

Efficient Defluorination: Application of Calcium Sulfate Precipitation Method in Zinc Sulfate Solution

Xiaoqing Zheng, Weiguang Zhang, Xuejiao Cao, Yibing Li, Xuexian Jiang,* Yang Chen, Yuping Li, and Tingan Zhang

Cite This: *ACS Omega* 2025, 10, 439−448

Read Online

ACCESS | Metrics & More | Article Recommendations

ABSTRACT: In the process of zinc hydrometallurgy, the content of fluorine in zinc sulfate solution directly affects the stripping of the zinc plate, which easily leads to the deterioration of working conditions. It not only has a serious impact on the entire zinc hydrometallurgical system but also causes huge economic losses. Especially in the process of zinc secondary resource utilization, the concentration of fluoride ions in the electrolyte exceeds the control standard of smelting enterprises, which has become a long-term technical challenge in the smelting industry. So far, no efficient and economical solution has been developed to effectively remove fluoride from a zinc sulfate solution with a high fluorine content. In view of this background, this study focuses on the application of the precipitation method, which stands out for its wide adaptability, simple operation, and cost advantages. The thermodynamic analysis of the purification and defluorination process of zinc sulfate solution was carried out, and the effects of different experimental conditions on the purification and defluorination of zinc sulfate solution were systematically explored. The results showed that when the solution was acidic, only a fluorite precipitated phase was formed in the system. In order to make the system only form a fluorite precipitated phase, the pH of the solution should be controlled below 7. Under the conditions of the molar ratio of Ca/F_2 is 1, the reaction time is 45 min, the solution pH is 4.5, the reaction temperature is 24 °C, and the stirring speed of 900 r min^{-1}, the fluorine removal rate can reach 83.19%, and the zinc loss rate is about 2%.

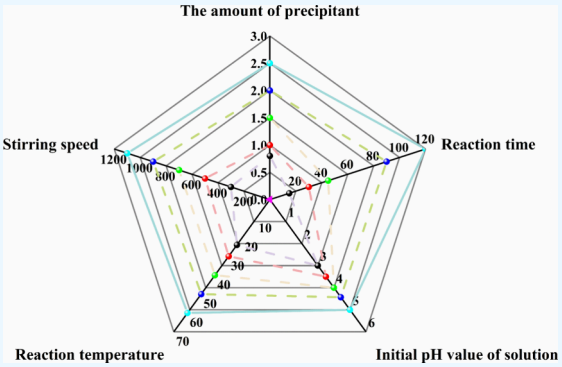

1. INTRODUCTION

Zinc is a metal widely used in the modern industry. Because of its excellent corrosion resistance, about half of zinc consumption is used for galvanizing, which is widely used in automobile, construction, shipbuilding, and other industries. In addition, zinc alloy has good processability and is often used in machinery manufacturing and battery making.

At present, the metal zinc produced by the hydrometallurgy process accounts for more than 80% of the total zinc output in the world. Hydrometallurgy process mainly includes four stages: roasting, leaching, purification, and electrowinning.[1] During the leaching process, impurities in the raw materials are dissolved in the leaching solution together with zinc, while fluoride exists in the solution in the form of ions. Some metal impurities can be removed by zinc powder replacement, while nonmetallic impurities such as chlorine and fluorine are easy to accumulate in the closed cycle of the solution, accelerating the corrosion of the cathode plate, affecting the stripping of zinc sheets, and in serious cases, "burning" will occur, which will interfere with the mechanized production of zinc hydrometallurgy enterprises, and cause great economic losses.[2−6] Moreover, with the substantial growth of zinc demand, the capacity growth of zinc concentrate can no longer meet the needs of enterprises. Secondary resources of zinc, such as arc furnace dust, blast furnace gas ash (mud), secondary zinc oxide dust, and so on, have become important raw materials for zinc smelting.[5,7] These secondary resources containing zinc have complex components, especially the high fluorine content, which inevitably leads to the excessive fluoride ion content in the electrolyte.[8]

However, zinc smelting enterprises have strict requirements on fluorine content, usually requiring that the fluorine content in zinc leaching solution be less than 50 mg/L.[9] Therefore, the exploration of efficient and economic fluoride removal methods has become the focus of the smelting industry.

At present, the methods for defluorination of zinc containing solution mainly include adsorption[10−12] chemical precipita-

Received: July 18, 2024
Revised: December 4, 2024
Accepted: December 12, 2024
Published: December 27, 2024

© 2024 The Authors. Published by American Chemical Society

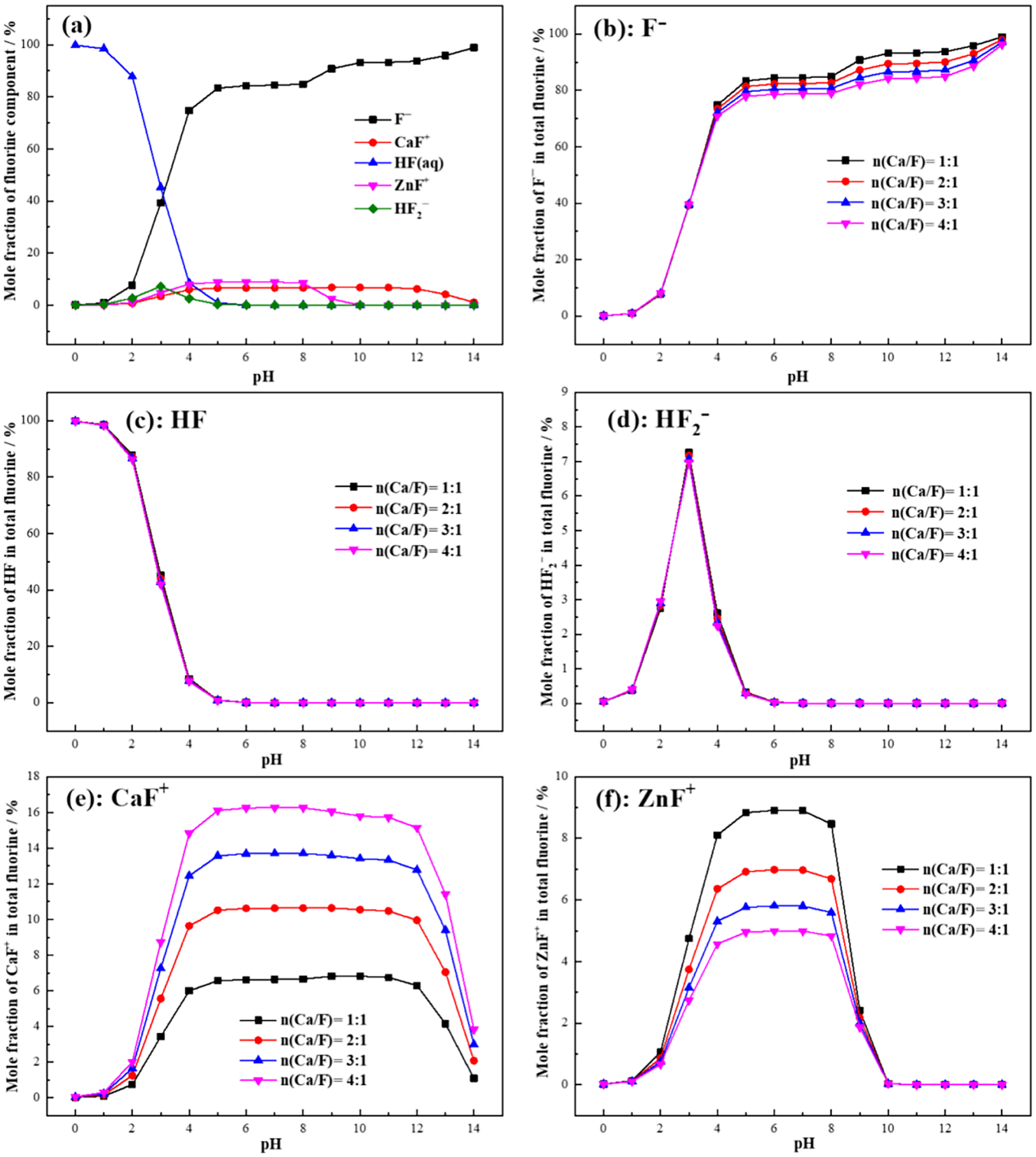

Figure 1. Mole fraction diagram of various fluoride ions. (a) All fluorine-containing components (Ca/F = 1:1), (b) F^- ion, (c) HF, (d) HF_2^- ion, (e) CaF^+ ion, and (f) ZnF^+ ion.

tion,[13−15] ion exchange,[16,17] electrochemical method,[18,19] etc. Bazrafshan[20] investigated the ability of $ZnCl_2$-treated eucalyptus leaves (70% dry leaves and 30% $ZnCl_2$) to act as a natural adsorbent for fluoride removal from synthetic solutions. However, in the wet zinc smelting system, this is due to the influence of sulfate ions and acidity in the zinc sulfate solution. The adsorption method has the problems of unstable defluorination effect, high loss rate of valuable metals, and low defluorination rate. Nalan[21] adopted electrodialysis to remove fluoride from aqueous solutions. Applied voltage, feed flow rate, fluoride concentration in the solution, and effect of the other anions as sulfate and chloride were investigated as experimental parameters on fluoride removal from aqueous solution. The separation performance was evaluated in terms of the mass transfer and energy consumption. It was obtained that the separation performance increased when the initial

https://doi.org/10.1021/acsomega.4c06641
ACS Omega 2025, 10, 439−448

concentration of fluoride in the feed solution increased. Percent removal of fluoride increased as the applied potential increased. Electrodialysis defluorination process is simple, with high treatment efficiency, but the cost is relatively high.

Compared with traditional methods, the advantages of precipitation method are wide adaptability, simple operation, and low cost.[22] In order to effectively solve the problem of economic and effective defluorination of zinc containing leaching solution, this paper proposes to use cheap calcium sulfate for the defluorination of high fluoride solution. At the same time of efficient defluorination, zinc loss shall be minimized to reduce the metal loss caused by defluorination. In this paper, the performance and mechanism of removing fluoride from zinc electrolytic solution by the precipitation method were studied.

2. EXPERIMENTAL SECTION

2.1. Materials. All of the reagents were analytical grade reagents, including sulfuric acid (H_2SO_4), sodium hydroxide (NaOH), calcium sulfate ($CaSO_4$), zinc sulfate heptahydrate ($ZnSO_4{\cdot}7H_2O$), and sodium fluoride (NaF), used for precipitation reaction.

The fluorine-containing zinc sulfate solution for the experiment was prepared by dissolving quantitative zinc sulfate heptahydrate and sodium fluoride in deionized water. The deionized water used in the experiments was produced with a water purification system.

2.2. Apparatus and Procedures. First, the mixed ion solution containing 120 $g{\cdot}L^{-1}$ Zn^{2+} and 1 $g{\cdot}L^{-1}$ F^- was prepared by quantitative zinc sulfate heptahydrate and sodium fluoride. Then, 150 mL of the solution was added to the polytetrafluoroethylene beaker and placed on a constant temperature magnetic stirrer for stirring. Subsequently, the pH value of the solution was adjusted with sulfuric acid and sodium hydroxide. Heat the solution to a predetermined temperature. Finally, calcium sulfate was added to the beaker and fully stirred to produce a uniform solution. After the required reaction time has passed, the filtrate is separated from the precipitate by vacuum filtration.

The change of pH value in the system was measured by a PHS-3F pH meter. The concentration of zinc ions in the solution was determined by a full spectrum direct reading plasma emission spectrometer (ICP). The concentration of fluoride ion in the filtrate was determined by a fluoride ion selective electrode method in a ZDJ-5B automatic potentiometric titrator. The defluorination ratio (η_1) and zinc loss rate (η_2) are calculated using the following formula:

$$\eta_1 = \frac{(C_1 \times V_1 - C_2 \times V_2)}{C_1 \times V_1} \times 100\% \quad (1)$$

$$\eta_2 = \frac{(C_3 \times V_1 - C_4 \times V_2)}{C_3 \times V_1} \times 100\% \quad (2)$$

where η_1 is the defluorination ratio, %; C_1 is the total fluorine concentration in the fluorine-containing zinc sulfate solution, $g{\cdot}L^{-1}$; V_1 is the volume of fluorine-containing zinc sulfate solution, mL; C_2 is the total fluorine concentration in the filtrate after precipitation reaction, $g{\cdot}L^{-1}$; and V_2 is the volume of filtrate after reaction, mL.

η_2 is the dezincification rate, %; C_3 is the total zinc concentration in zinc sulfate solution containing fluorine, $g{\cdot}L^{-1}$; and C_4 is the total zinc concentration in the filtrate after the precipitation reaction, $g{\cdot}L^{-1}$.

Characterization instrument: D8 ADVANCE X-ray diffractometer (Bruker GmbH, Germany) and Nicolet 6700 FT-IR Spectrometer (Thermo Fisher Scientific, USA).

3. RESULTS AND DISCUSSION

3.1. Thermomechanical Analysis. *3.1.1. Concentration Distribution of Fluorine Component in the Ca^{2+}–Zn^{2+}–H^+–F^-–SO_4^{2-} Solution.* During the defluoridation process by using calcium sulfate in zinc sulfate solution, the following chemical reaction formulas 3–6 exist. Fluorine in solution exists in the forms of F^-, HF, HF_2^-, CaF^+, and ZnF^+. The software of Visual MINTEQ was used for thermodynamic analysis. The fluoride concentration was set at 0.05 $mol{\cdot}L^{-1}$(1 $g{\cdot}L^{-1}$). The amount of calcium sulfate was 1, 2, 3, and 4 times the theoretical amount; that is, the concentration of calcium ion was 0.025, 0.05, 0.075, and 0.10 $mol{\cdot}L^{-1}$.

$$H^+ + F^- = HF \quad (3)$$

$$HF + F^- = HF_2^- \quad (4)$$

$$Ca^{2+} + F^- = CaF^+ \quad (5)$$

$$Zn^{2+} + F^- = ZnF^+ \quad (6)$$

The mole fractions of various soluble fluorine ions in total fluorine are shown in Figure 1.

Observing Figure 1a, it can be seen that when the amount of calcium sulfate added reaches the theoretical amount, the pH value ranges between 3 and 5. Fluoride mainly exists in the solution as HF and F^-, with trace amounts of HF^{2-}, CaF^+, and ZnF^+. As the pH increases, HF in the solution gradually converts to F^-. Figure 1b shows that the molar percentage of F^- increases with the pH value, rising from 0% at pH 0 to 1 to 80% at pH 4 to 5, and approaching 100% at pH 14. Additionally, as the Ca/F molar ratio increases from 1 to 4, the molar percentage of F^- decreases due to the excess calcium ions combining with F^- to form CaF^+.

Figure 1c reveals that the molar percentage of HF decreases with the rise in pH, dropping from 100% at pH 0 to 1 to 0% at pH 5 and maintaining this level at pH 14. The change in the Ca/F molar ratio has little effect on the molar percentage of HF, likely because fewer fluoride complexes form in the acidic environment of pH 0–4. Figure 1d indicates that the molar percentage of HF^{2-} reaches a maximum of only 7% (at pH 3) within the pH range of 1–5, and the increase in the Ca/F molar ratio has minimal impact on its molar percentage.

Figure 1e reflects that the molar percentage of CaF^+ initially rises with the increase in pH (from pH 0 to 5), stabilizes from pH 5 to 11, and finally declines from pH 11 to 14. The initial rise is due to the enhanced complexation ability of F^- with calcium ions, while the decline results from the relatively stronger complexation ability of calcium ions with hydroxide ions, leading to the conversion of CaF^+ to F^- and $Ca(OH)^+$.[23] With the increase in the Ca/F molar ratio, the molar percentage of CaF^+ during the stable phase increases from 6 to 16%, indicating that excess calcium ions combine with more F^-. Figure 1f shows that the molar percentage of ZnF^+ exhibits a trend similar to that of CaF^+, rising with the increase in pH (from pH 0 to 5), stabilizing between pH 5 and 7, and then decreasing from pH 7 to 10, ultimately reaching 0% at pH 10–14. This trend is consistent with the reasons for the changes in CaF^+. As the Ca/F molar ratio increases, the molar percentage

https://doi.org/10.1021/acsomega.4c06641
ACS Omega 2025, 10, 439–448

of ZnF^+ during the stable phase decreases from 9 to 5%, indicating that the complexation ability of fluoride with calcium ions is stronger than with zinc ions.

3.1.2. Concentration Distribution of Zinc Component in the Ca^{2+}–Zn^{2+}–H^+–F^-–SO_4^{2-} Solution. There are the following chemical reaction eqs 6–12 in the calcium defluorination system: the main existing forms of zinc in zinc sulfate solution in calcium sulfate defluorination system are Zn^{2+}, ZnF^+, $ZnSO_4(aq)$, $ZnOH^+$, $Zn(OH)_2(aq)$, $Zn(OH)_3^-$, $Zn(OH)_4^{2-}$, $Zn_2(OH)_3^+$, and $Zn(SO_4)_2^{2-}$. When the molar ratio of Ca/F_2 is 1:1, the variation trend of the zinc component mole fraction with pH is shown in Figure 2.

$$Zn^{2+} + SO4^{2-} = ZnSO_4 \quad (7)$$

$$Zn^{2+} + OH^- = ZnOH^+ \quad (8)$$

$$Zn^{2+} + 2OH^- = Zn(OH)_2 \quad (9)$$

$$Zn^{2+} + 3OH^- = Zn(OH)_3^- \quad (10)$$

$$Zn^{2+} + 4OH^- = Zn(OH)_4^{2-} \quad (11)$$

$$2Zn^{2+} + 3OH^- = Zn_2(OH)^{3+} \quad (12)$$

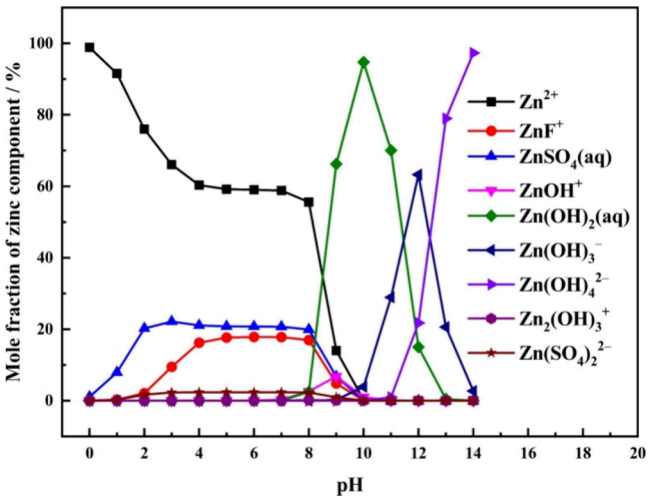

Figure 2. Mole fraction of various zinc components in solution.

Figure 2 illustrates that when the pH of the solution is between 3 and 5, zinc primarily exists as Zn^{2+}, ZnF^+, and $ZnSO_4(aq)$, with zinc ions accounting for approximately 60% of the total zinc content, while ZnF^+ and $ZnSO_4(aq)$ each constitute about 20%. As the pH of the solution increases, particularly beyond pH 8, the proportions of Zn^{2+}, ZnF^+, and $ZnSO_4(aq)$ decrease significantly, and zinc begins to complex with OH^- ions, forming species such as $Zn(OH)_2$, $Zn(OH)^{3-}$, and $Zn(OH)_4^{2-}$.

Given that the zinc sulfate solution is an acidic system during the calcium-based defluorination process, the focus of the study is on the variation of Zn^{2+}, ZnF^+, and $ZnSO_4(aq)$ with pH.

Figure 3 depicts the variation in the molar percentages of Zn^{2+}, ZnF^+, and $ZnSO_4(aq)$ in the total zinc content with increasing Ca/F molar ratios. This indicates that changes in the Ca/F molar ratio significantly affect the forms in which zinc exists, a trend that is crucial for optimizing the defluorination process and understanding the chemical reactions in the solution.

According to Figure 3a, the increase in the solution's pH leads to a two-stage change in the molar percentage of Zn^{2+}: it decreases slowly from pH 0 to 8 and then drops sharply to zero from pH 8 to 10. This gradual decline is attributed to the complexation of Zn^{2+} with F^- and SO_4^{2-} ions, forming ZnF^+ and $ZnSO_4(aq)$ (see Figure 3b,c). The sharp decline is due to the binding of Zn^{2+} with OH^- ions, resulting in various zinc hydroxide complexes (see Figure 2). Additionally, as the Ca/F molar ratio increases with more calcium sulfate added, the molar percentage of Zn^{2+} continues to decrease because the dissolution of calcium sulfate raises the concentration of SO_4^{2-} in the solution, promoting the transformation of Zn^{2+} to $ZnSO_4(aq)$. Figure 3b shows the variation in the molar percentage of ZnF^+ with solution pH and Ca/F molar ratio, consistent with the pattern shown in Figure 1e, and the reasons are identical, so they are not repeated here.

Figure 3c reveals the changes in the molar percentage of $ZnSO_4(aq)$ with increasing pH: it rises from pH 0 to 2, remains stable from pH 2 to 8, sharply declines from pH 8 to 10, and drops to zero from pH 10 to 14. In the Ca^{2+}–Zn^{2+}–H^+–F^-–SO_4^{2-} solution system, there are three kinds of zinc ion complexation reactions, including Zn^{2+} and F^-, Zn^{2+} and $SO4^{2-}$, and Zn^{2+} and OH^-, in which the complexation equilibrium constant of Zn^{2+} and $SO4^{2-}$ is the smallest. When the pH value is 2–8, there is mainly the complexation of Zn^{2+} and F^-, mainly the reaction of Zn^{2+} to ZnF^+, that is, the concentration of Zn^{2+} is decreasing and the concentration of ZnF^+ is increasing, so the concentration of $ZnSO_4(aq)$ is almost unchanged in this process. The increase in the $ZnSO_4(aq)$ molar percentage is due to the complexation of Zn^{2+} with SO_4^{2-} to form $ZnSO_4(aq)$, while the decline is caused by the formation of zinc hydroxide complexes with OH^-. Furthermore, the molar percentage of $ZnSO_4(aq)$ also shows an upward trend with the increasing Ca/F molar ratio, consistent with the previously discussed reasons for the decrease in the zinc ion concentration.

At pH = 6 and $n(Ca/F)$ = 1:1, the sum of the percentages of Zn^{2+}, ZnF^+, and $ZnSO_4$ is about 100%. However, at pH = 6 and $n(Ca/F)$ = 4:1, the sum of the percentages of Zn^{2+}, ZnF^+, and $ZnSO_4$ is only about 90%. This is because Figure 3 shows the concentration variation of the three main zinc containing components with the change of pH value under different calcium–fluorine molar ratios. According to Figure 2, in addition to the three main zinc containing components, there are other types: $ZnOH^+$, $Zn(OH)_2(aq)$, $Zn(OH)_3^-$, $Zn(OH)_4^{2-}$, $Zn_2(OH)_3^+$, and $Zn(SO_4)_2^{2-}$. Therefore, the sum of the molar concentration ratio of the three is not necessarily 1.

3.1.3. Precipitate Phase in the Ca^{2+}–Zn^{2+}–H^+–F^-–SO_4^{2-} Solution. In the process of thermodynamic analysis by Visual MINTEQ, the saturation index SI can be used to predict the trend of precipitation and dissolved substances and is calculated by formula 7. When SI < 0, the phase exists in the solution in the form of ions; when SI > 0, the phase may exist in the solution in the form of precipitation; and when SI = 0, the phase reaches the equilibrium of dissolution and precipitation.

When the mole fraction of Ca/F_2 is 1, the precipitation phase that may exist in the zinc sulfate solution is predicted by Visual MINTEQ software, and the calculation results are shown in Figure 4

https://doi.org/10.1021/acsomega.4c06641
ACS Omega 2025, 10, 439–448

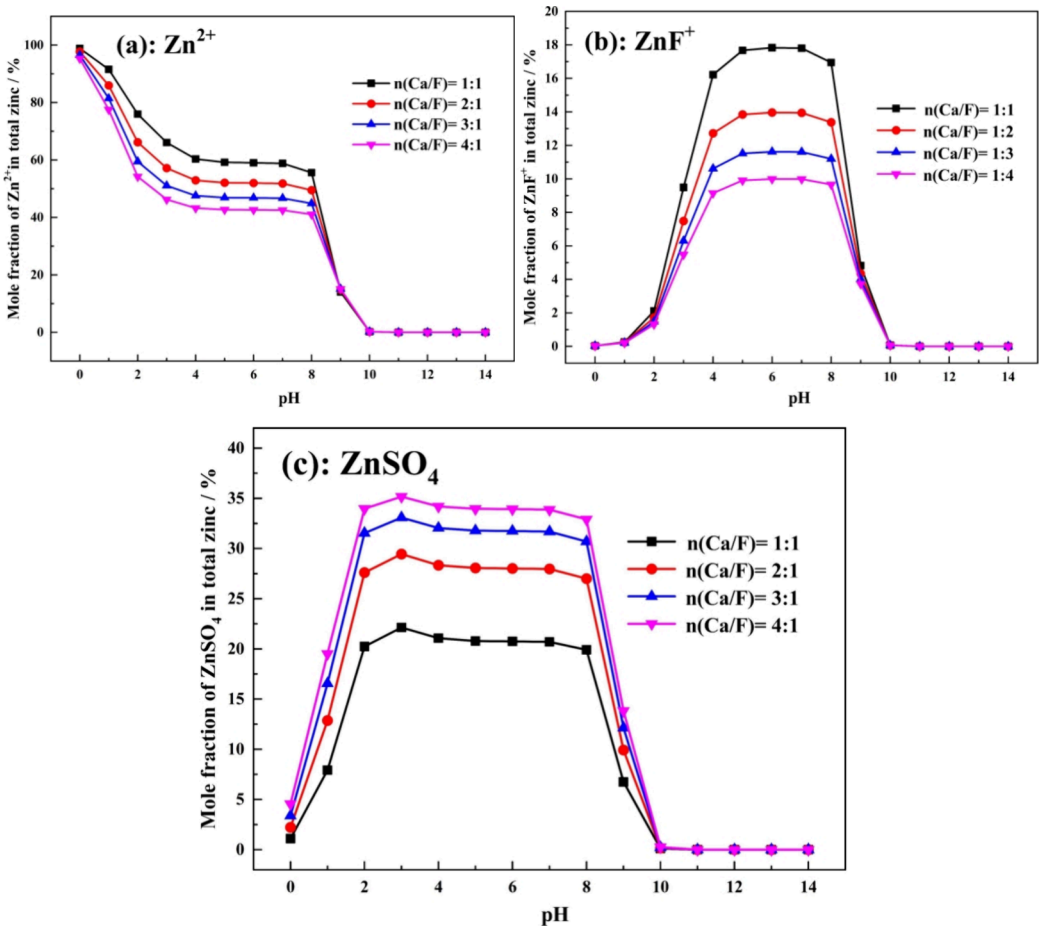

Figure 3. Mole fraction of Zn^{2+}, ZnF^{+}, and $ZnSO_4$(aq) in total zinc ions under different Ca/F ratios. (a) Zn^{2+} ion, (b) ZnF^{+} ion, and (c) $ZnSO_4$(aq).

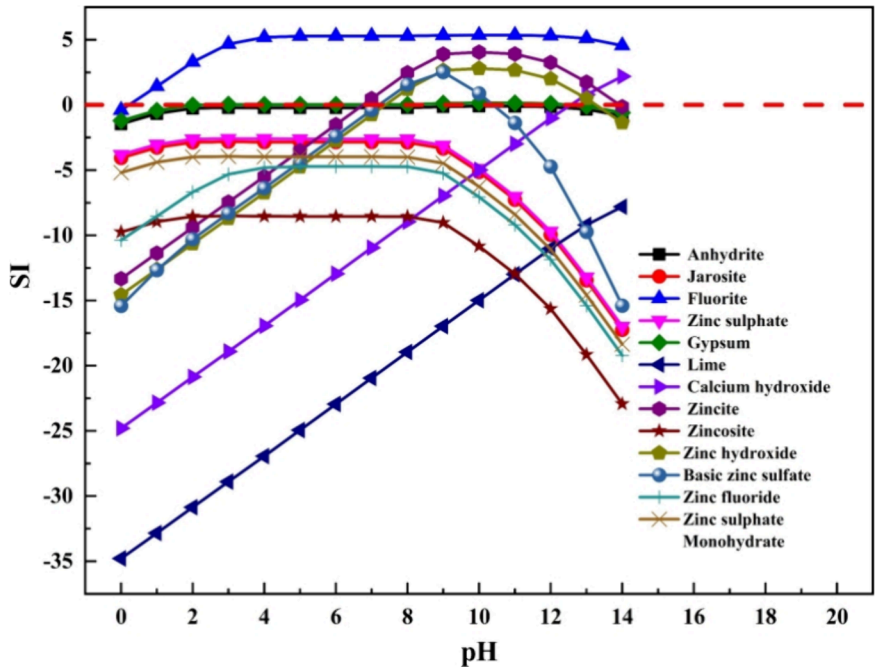

Figure 4. Saturation index of each substance under different pH values.

$$SI = \log IAP - \log K_s \quad (13)$$

Here, IAP is the selected ionic activity in Visual MINTEQ software; K_s is the solubility product constant.

https://doi.org/10.1021/acsomega.4c06641
ACS Omega 2025, 10, 439−448

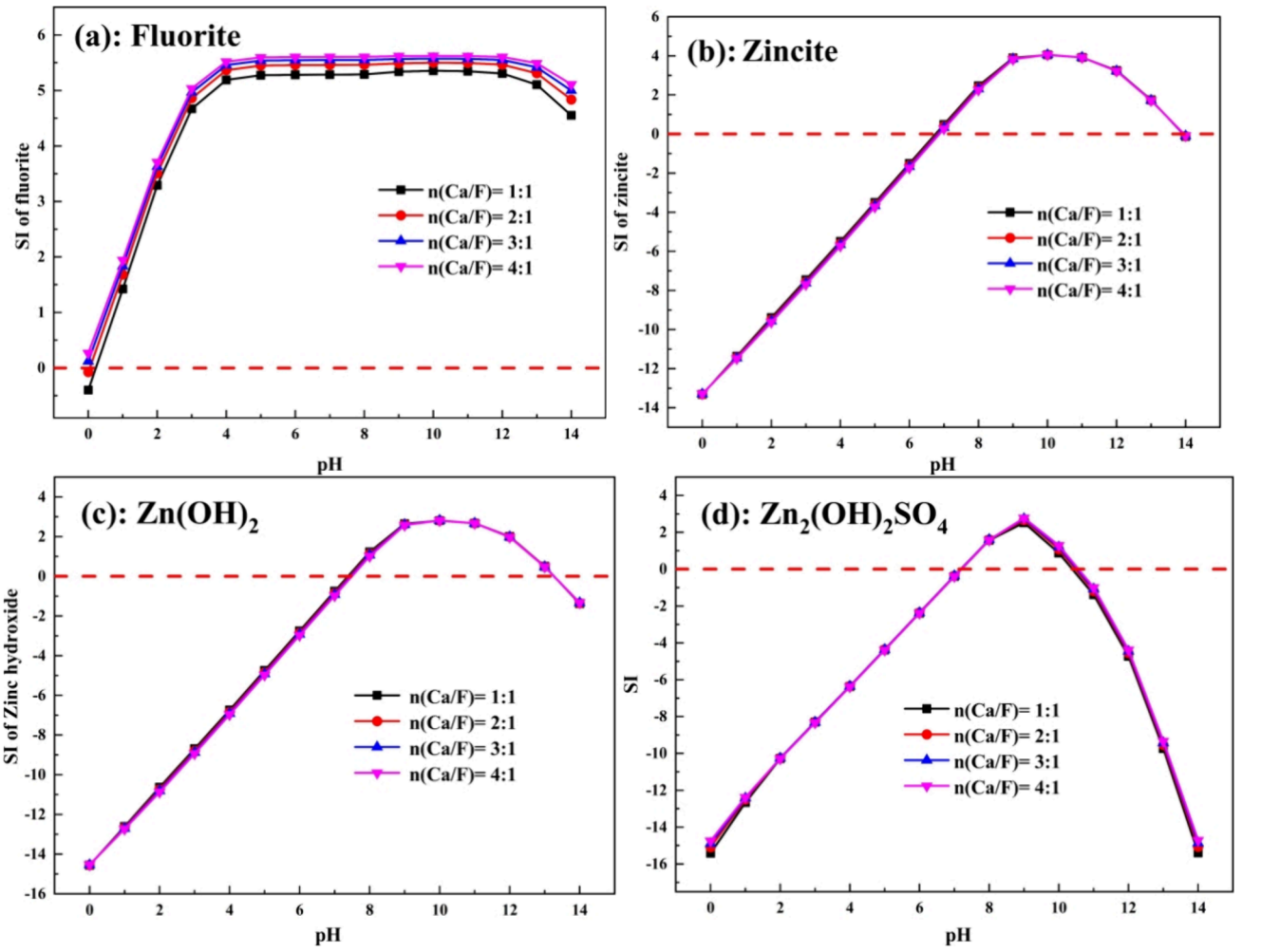

Figure 5. Saturation index of four precipitation phases under different Ca/F ratios. (a) Fluorite, (b) zincite, (c) $Zn(OH)_2$, and (d) $Zn_2(OH)_2SO_4$.

Observing Figure 4, it can be seen that the fluorite (fluorspar) precipitate phase remains stable in both acidic and alkaline environments. In acidic solutions, fluorite is the primary precipitate formed. However, when the pH of the solution rises to the range of 8−12, in addition to fluorite, precipitate phases such as zincite, zinc hydroxide, and basic zinc sulfate also appear. To ensure that only fluorite precipitates in the system, the pH of the solution needs to be maintained below 7. Figure 5 shows the changes in the saturation index (SI) values of the four precipitate phases with an increasing Ca/F molar ratio. The results indicate that the increase in Ca/F molar ratio has little effect on the SI values of these four precipitate phases, implying that the formation of the precipitate phases is not significantly related to the Ca/F molar ratio.

3.2. Experimental Study on Defluorination with Calcium Sulfate. *3.2.1. Effect of the Amount of Precipitant.* The effects of different Ca/F molar ratios on defluorination were investigated, and the analysis results are shown in Figure 6 and Table 1.

Figure 6 shows the effect of the amount of calcium sulfate on the defluorination rate. As the amount increases, the defluorination rate rises from 60.40 to 81.98% and then stabilizes. This phenomenon aligns with the thermodynamic analysis results in Section 3.1. At pH 4.33, some fluoride forms CaF^+ and ZnF^+, making it more difficult to completely remove fluoride from the solution. Throughout the precipitation process, the zinc loss rate remains below 1%, mainly due to mechanical encapsulation. Therefore, the optimal Ca/F molar ratio for defluorination with calcium sulfate is determined to be 1.

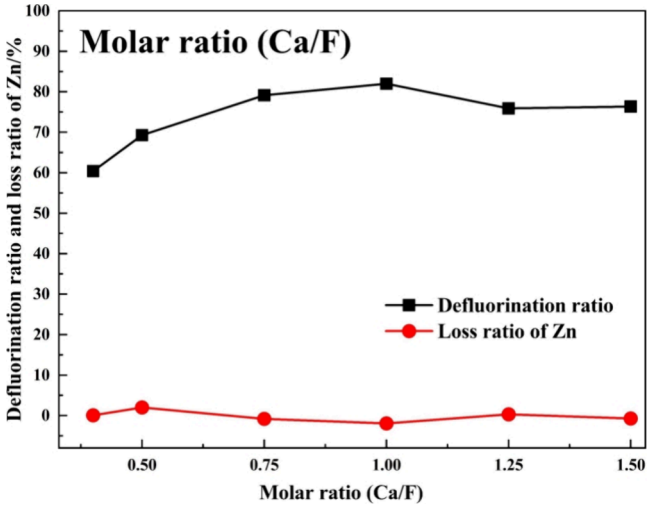

Figure 6. Influence of the amount of precipitant on the efficiency of fluorine removal.

https://doi.org/10.1021/acsomega.4c06641
ACS Omega 2025, 10, 439−448

Table 1. Variation of pH before and after the Reaction

subsidence ratio	0.8	1.0	1.5	2.0	2.5
the pH value of stock solution	4.33	4.33	4.33	4.33	4.33
the pH value of the solution after precipitation	4.31	4.30	4.27	4.40	4.23
the concentration of Ca^{2+} after precipitation/mg·L^{-1}	54.60	128	530	525	505

The data in Table 1 reveal minor changes in the solution pH before and after the reaction. As the amount of calcium sulfate increases, the concentration of calcium ions in the precipitated solution rises due to the formation of CaF^+ from the combination of calcium ions and fluoride ions, which increases the calcium ion concentration in the solution. This observation is consistent with the thermodynamic analysis results shown in Figure 1.

3.2.2. Effect of Reaction Time. The effect of different reaction times on defluorination efficiency was analyzed, and the results are presented in Figure 7 and Table 2. Figure 7

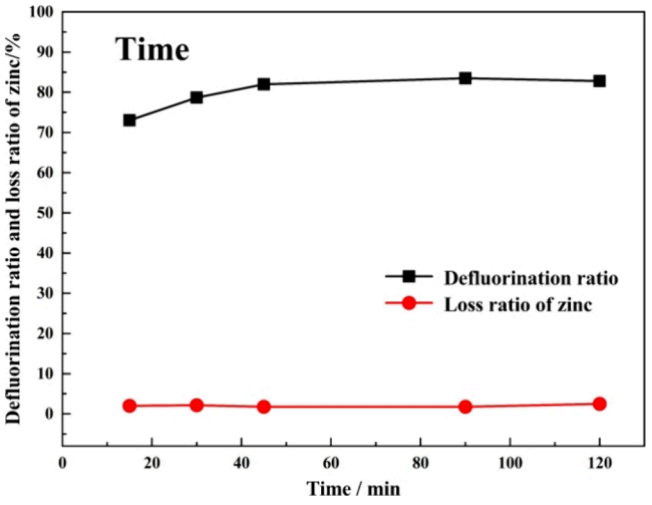

Figure 7. Influence of time on the efficiency of fluorine removal.

Table 2. Variation of pH before and after the Reaction

time/min	15	30	45	90	120
the pH value of stock solution	4.51	4.47	4.34	4.40	4.41
the pH value of the solution after precipitation	4.25	4.25	4.40	4.29	4.23
the concentration of Ca^{2+} after precipitation/mg·L^{-1}	535	536	545	550	545

indicates that as the reaction time increases, the defluorination rate of the solution initially rises and then slightly decreases. This decrease might be due to the redissolution of calcium fluoride with prolonged reaction time. Throughout the experiment, the zinc loss rate remains low, around 2%, primarily due to mechanical entrapment during the precipitation process. Considering all factors, the optimal reaction time for the purification and defluorination of fluoride-containing zinc sulfate solution using calcium sulfate is determined to be 45 min.

Table 2 variation of pH before and after the reaction shows that the pH value of the solution after precipitation slightly decreases compared to before the reaction, and different reaction times have minimal impact on the pH value. Additionally, the calcium ion concentration in the solution after precipitation does not significantly change with the extended reaction times.

3.2.3. Effect of Initial pH Value of Solution. The impact of initial pH on defluorination efficiency was investigated, and the results are displayed in Figure 8 and Table 3. Figure 8 reveals

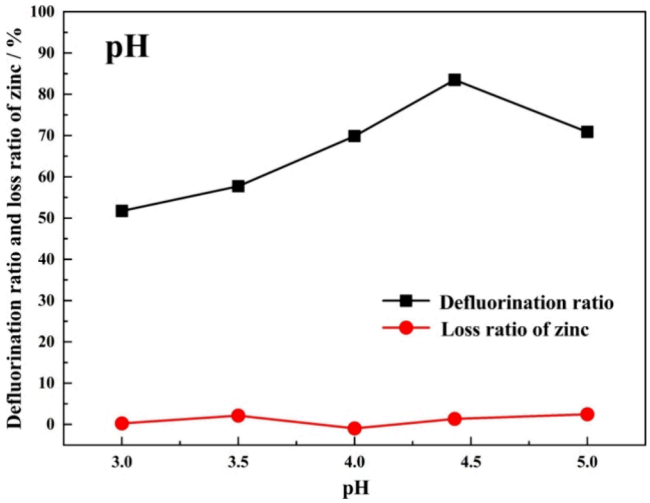

Figure 8. Influence of pH on the efficiency of fluorine removal.

Table 3. Variation of pH before and after the Reaction

time/min	90	90	90	90	90
the pH value of stock solution	3.0	3.5	4.0	4.43	5
the pH value of the solution after precipitation	2.64	3.08	3.63	4.40	4.94
the concentration of Ca^{2+} after precipitation/mg·L^{-1}	500	500	504	490	540

the effect of solution pH on the fluoride removal efficiency. Initially, at a pH of 3.0, the defluorination rate is 51.72%. As the pH increases, the defluorination rate significantly improves, reaching 83.49% at a pH of 4.43. However, when the pH further increases to 5, the defluorination rate drops to 70.86%. This decline may be due to the higher proportion of CaF^+ and ZnF^+ complex ions formed at this pH, which hinders fluoride removal. Throughout the pH study range, the zinc loss rate remains low, around 2%, primarily caused by mechanical entrapment during the precipitation process. Therefore, the defluorination pH of calcium sulfate in a zinc sulfate solution should be controlled between 4.0 and 5.0.

The data in Table 3 indicate that the pH of the solution decreases after precipitation, and the calcium ion concentration in the solution after precipitation does not significantly change with different reaction times.

3.2.4. Effect of Reaction Temperature. Temperature, as a key factor, significantly influences chemical reactions, altering the solubility of substances in solution and their states of supersaturation. This study investigated the effect of reaction temperature on defluorination efficiency, and the relevant analysis results are presented in Figure 9 and Table 4 variation of pH before and after the reaction

According to the observations in Figure 9, within the temperature range examined, the defluorination efficiency did not exhibit significant fluctuations with increasing temperature. Specifically, when the temperature was maintained between 24 and 40 °C, the defluorination efficiency stabilized at approximately 83%. As the temperature increased to 50 °C,

https://doi.org/10.1021/acsomega.4c06641
ACS Omega 2025, 10, 439−448

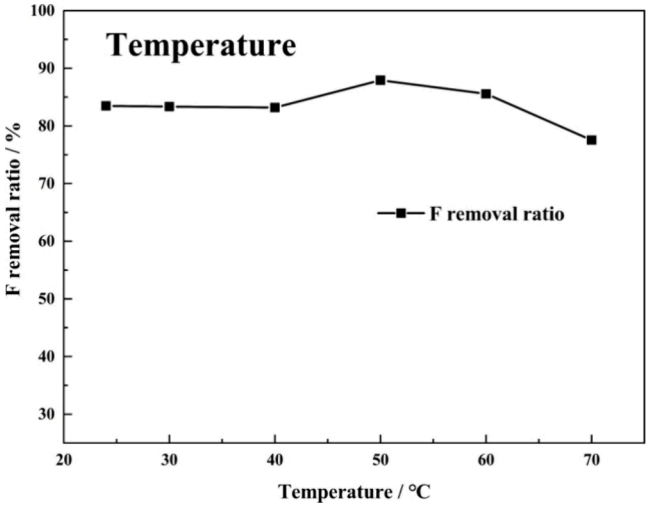

Figure 9. Influence of temperature on the efficiency of fluorine removal.

Table 4. Variation of pH before and after the Reaction

temperature/°C	normal temperature	30	40	50	60	70
the pH value of stock solution	4.40	4.17	4.16	4.15	4.14	4.16
the pH value of the solution after precipitation	4.29	3.88	3.85	3.80	3.71	3.74
the concentration of Ca^{2+} after precipitation/ $mg{\cdot}L^{-1}$	525	570	500	540	796	350

the defluorination efficiency slightly increased to 87.93%. However, with a further increase in temperature to 60 °C, the defluorination efficiency slightly decreased to 85.57%. When the temperature continued to rise to 70 °C, the defluorination efficiency decreased to 77.54%. As the temperature increases, there is no significant change in the defluorination rate. This is because the defluorination mechanism in sulfuric acid solution utilizes the small solubility product of calcium fluoride (K_{sp} = 2.7 × 10^{-11}[24]), which does not vary significantly with temperature. Considering energy consumption, 24 °C is considered the optimal defluorination temperature.

The data in Table 4 variation of pH before and after the reaction reveal that the pH of the solution decreases after the reaction compared to before, and the decrease in pH becomes more significant with increasing temperature. Furthermore, the concentration of calcium ions in the solution after precipitation remains at approximately 500 $mg{\cdot}L^{-1}$. At 60 °C, the concentration of calcium ions in the defluorinated solution is higher than 500 $mg{\cdot}L^{-1}$, which may be related to the lower pH value of the defluorinated solution (pH is 3.71 lower than the pH value of the defluorinated solution at other temperatures). When the acidity is higher, the higher the hydrogen ion concentration, the more fluorine forms HF (aq) (Figure 1a,c), resulting in a decrease in the defluorination rate and a corresponding increase in the concentration of calcium ions in the defluorinated solution.

3.2.5. Effect of Stirring Speed. The influence of stirring speed on defluorination efficiency was analyzed, and the results are presented in Figure 10 and Table 5 variation of pH before and after the reaction

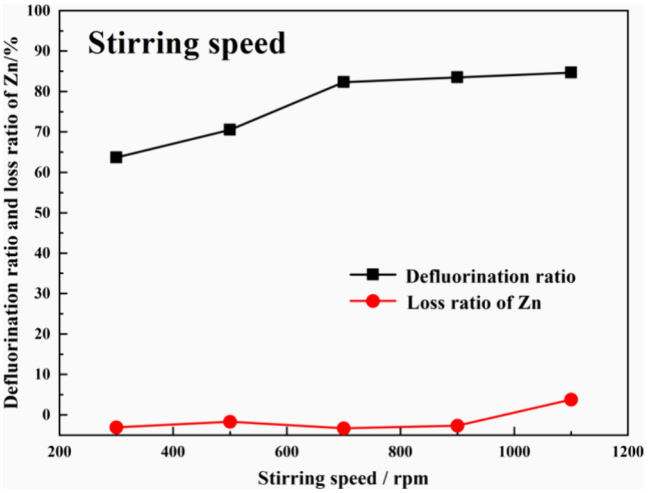

Figure 10. Influence of stirring speed on the efficiency of fluorine removal.

Table 5. Variation of pH before and after the Reaction

stirring speed/$r{\cdot}min^{-1}$	300	500	700	900	1100
the pH value of stock solution	4.51	4.50	4.52	4.40	4.50
the pH value of the solution after precipitation	4.44	4.45	4.43	4.29	4.46
the concentration of Ca^{2+} after precipitation/$mg{\cdot}L^{-1}$	540	542	548	536	530

Figure 10 demonstrates that with an increase in stirring speed, the removal rate of fluoride also increases. When the stirring speed reaches 900 rpm, the removal rate of fluoride reaches 83.19%. Further increasing the speed to 1100 rpm, the removal rate increases to 84.66%. This phenomenon can be explained by the formation of insoluble calcium fluoride on the surface of gypsum particles after gypsum addition, which encapsulates the gypsum particles, hindering further reaction. Strengthening the stirring can disrupt this surface encapsulation layer, allowing the encapsulated gypsum to participate more effectively in the reaction, thereby enhancing the defluorination efficiency. From an energy consumption perspective, 900 rpm is determined to be the optimal stirring speed. Throughout the experiment, the zinc loss rate remains approximately 2%.

The data in Table 5 indicate that the pH of the solution decreases after the reaction compared to before, while the concentration of calcium ions in the solution remains approximately 540 mg per liter (mg/L). This suggests that the increase in stirring speed did not have a significant effect on the pH value and calcium ion concentration in the solution.

3.3. XRD and IR. The precipitation products under the optimal experimental conditions were analyzed by XRD (X-ray diffraction). Figure 11 shows the XRD pattern of the precipitate. The results show that the X-ray diffraction peaks of the precipitate products are in one-to-one correspondence with the peak positions of the standard PDF card of CaF_2 (PDF#65-0535, space group: $Fm3m$[25]), and there is no impurity phase or second phase.

Figure 12 shows the infrared spectrum of the precipitated product under the optimum experimental conditions. The characteristic absorption peak of the precipitate is located at 1081.56 cm^{-1}, which is consistent with the transmission wavelength of CaF_2 in the standard infrared absorption

https://doi.org/10.1021/acsomega.4c06641
ACS Omega 2025, 10, 439−448

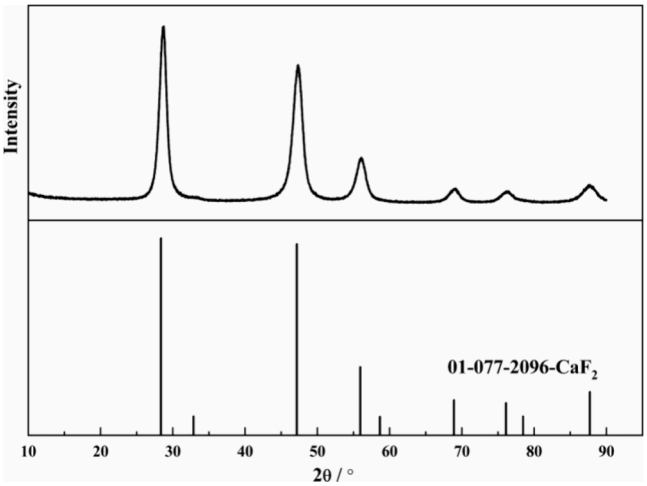

Figure 11. X-ray diffraction pattern of the precipitation.

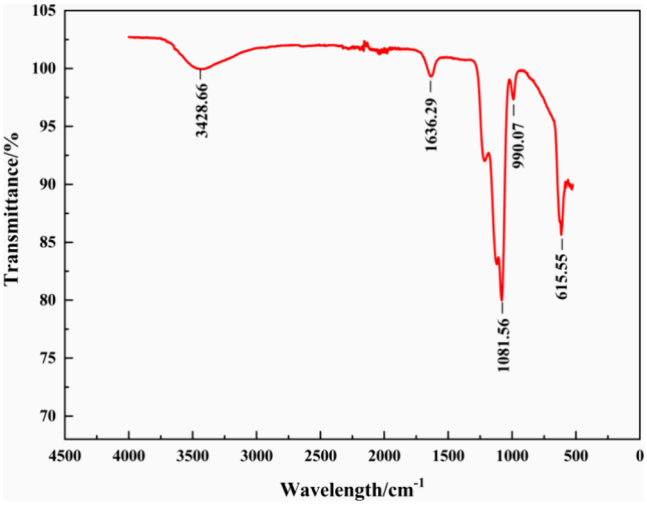

Figure 12. Infrared spectra of the precipitate.

spectrum of 1080 cm^{-1}.[26] The absorption peak at 3428.66 cm^{-1} is caused by the tensile vibration of O−H, which is caused by the inclusion of molecular water or hydroxyl water in fluorite.[27] The absorption peak of CaF_2 at 1636.29 cm^{-1} corresponds to the bending vibration peak of O−H.[28]

4. CONCLUSIONS

In this paper, thermodynamic analysis of the purification and defluorination of zinc sulfate solution was carried out, and the effects of different experimental conditions on the purification and defluorination of zinc sulfate solution were explored. The following conclusions were obtained.

1. Thermodynamic calculation results indicate that when the solution is acidic, the system only generates fluorite precipitated phase. In order to make the system only generate fluorite precipitated phase, the pH of the solution needs to be controlled below 7.
2. The experimental results of removing fluorine from zinc sulfate solution by gypsum method show that from the perspective of defluorination rate and zinc loss rate, the optimal experimental condition is that the molar ratio of Ca/F_2 is 1, the reaction time is 45 min, the solution pH is 4.5, the reaction temperature is 24 °C and the stirring speed is 900 $r \cdot min^{-1}$, the fluorine removal rate reached 83.19%, and the zinc loss rate was 2.67%.

AUTHOR INFORMATION

Corresponding Author

Xuexian Jiang − *Guilin University of Technology AT Nanning, Nanning, Guangxi 532100, China;* orcid.org/0009-0008-2049-0445; Phone: +86 13978855390; Email: 13978855390@163.com

Authors

Xiaoqing Zheng − *College of Materials Science and Engineering, Key Laboratory of New Technology for Non Ferrous Metals and Materials Processing, and Collaborative Innovation Center for Exploration of Nonferrous Metal Deposits and Efficient Utilization of Resources, Guilin University of Technology, Guilin, Guangxi 541004, China*

Weiguang Zhang − *College of Materials Science and Engineering, Key Laboratory of New Technology for Non Ferrous Metals and Materials Processing, and Collaborative Innovation Center for Exploration of Nonferrous Metal Deposits and Efficient Utilization of Resources, Guilin University of Technology, Guilin, Guangxi 541004, China*

Xuejiao Cao − *College of Materials Science and Engineering, Key Laboratory of New Technology for Non Ferrous Metals and Materials Processing, and Collaborative Innovation Center for Exploration of Nonferrous Metal Deposits and Efficient Utilization of Resources, Guilin University of Technology, Guilin, Guangxi 541004, China*

Yibing Li − *College of Materials Science and Engineering, Key Laboratory of New Technology for Non Ferrous Metals and Materials Processing, and Collaborative Innovation Center for Exploration of Nonferrous Metal Deposits and Efficient Utilization of Resources, Guilin University of Technology, Guilin, Guangxi 541004, China*

Yang Chen − *College of Materials Science and Engineering, Key Laboratory of New Technology for Non Ferrous Metals and Materials Processing, and Collaborative Innovation Center for Exploration of Nonferrous Metal Deposits and Efficient Utilization of Resources, Guilin University of Technology, Guilin, Guangxi 541004, China*

Yuping Li − *College of Materials Science and Engineering, Key Laboratory of New Technology for Non Ferrous Metals and Materials Processing, and Collaborative Innovation Center for Exploration of Nonferrous Metal Deposits and Efficient Utilization of Resources, Guilin University of Technology, Guilin, Guangxi 541004, China*

Tingan Zhang − *School of Materials and Metallurgy, Northeastern University, Shenyang, Liaoning 110004, China*

Complete contact information is available at: https://pubs.acs.org/10.1021/acsomega.4c06641

Notes

The authors declare no competing financial interest.

ACKNOWLEDGMENTS

This work was financially supported by the Guangxi Science and Technology Program Projects (Major Special Projects No.AA22068077), the Guangxi innovation-driven development special fund project (AA22068080), the Guangxi Science and Technology Program Projects (No. 2023GXNSFBA026140), the National Natural Science Foun-

https://doi.org/10.1021/acsomega.4c06641
ACS Omega 2025, 10, 439−448

dation of China (No. 52204358), the National Natural Science Foundation of China (No. 52464045) and the Guangxi Science and Technology Program Projects (Major Special Projects No. AA23023033).

REFERENCES

(1) Xu, Y.; Qu, D.; Xia, H.; Zhang, Q.; Zhang, L. Migration behavior of germanium and its related elements in zinc hydrometallurgy process. *Separation and Purification Technology.* **2024**, *330* (PB), No. 125467.
(2) Wang, H.; Liu, S. Removal of Fluorine and Chlorine from Zinc Solution. *Mining Metallurgy* **2017**, *26* (4), 49−52.
(3) Wang, W.; Chen, H.; Chen, S.; Wang, J.; Shu, J. Study on efficient defluorination process of sulfate solution in zinc hydrometallurgy. *World Nonferrous Met.* **2020**, *12*, 5−6.
(4) Yang, T.; Kong, J.; Zhang, X. Discussion on the method of removing fluorine and chlorine from zinc sulfate solution in zinc hydrometallurgy. *Nonferrous Metallurgy Energy Saving* **2018**, *34* (1), 30−33.
(5) Guo, T.; Wei, L. Development direction of the recycling industry of secondary zinc resources. *China Nonferrous Metallurgy* **2010**, *39* (6), 56−59.
(6) Yao, Y.; Chen, X.; Zhu, B.; Chen, G. Production practice of zinc hydrometallurgy with high fluorine and chlorine secondary zinc oxide dust. *China Nonferrous Metallurgy* **2019**, *48* (04), 24−28.
(7) Luo, Y.; Yuan, X.; Zhou, Y.; Ma, B.; Liao, Y.; Deng, Z. Recovery of zinc and lead from zinc suboxide bearing high fluorine and chlorine. *Nonferrous Met. (Extract. Metallurgy)* **2020**, *1*, 9−13.
(8) Tu, B.; Zhong, S.; Chen, H.; Chi, X.; Rao, F. Research status of fluorine removal technology in zinc hydrometallurgy system. *Met. Mine* **2022**, *05*, 103−110.
(9) Hu, X.; Peng, X.; Kong, L. Removal of fluoride from zinc sulfate solution by in situ Fe(III) in a cleaner desulfuration process. *Journal of Cleaner Production.* **2017**, *164*, 163−170.
(10) Mukherjee, S.; Halder, G. A review on the sorptive elimination of fluoride from contaminated wastewater. *Journal of Environmental Chemical Engineering.* **2018**, *6* (1), 1257−1270.
(11) Lee, J. I.; Hong, S. H.; Lee, C. G.; Park, S. J. Fluoride removal by thermally treated egg shells with high adsorption capacity, low cost, and easy acquisition. *Environ. Sci. Pollut. Res.* **2021**, *28* (27), 35887−35901.
(12) Mo, M.; Zeng, Q.; Li, M. Study of the fluorine adsorption onto zirconium oxide deposited strong alkaline anion exchange fiber. *J. Appl. Polym. Sci.* **2018**, *135* (7), 45855.
(13) Ling, J.; Qin, H.; Li, H. Study on the treatment of high concentration fluorine-containing wastewater by chemical precipitation method. *Petrochem. Technol.* **2011**, *18* (2), 9−11.
(14) Wang, Z.; Xu, S.; Xu, H.; Peng, S.; Kuang, J.; Xie, W.; Deng, Y. Orthogonal test of calcium hydroxide precipitation method for the treatment of acidic fluorine-containing wastewater purified from microcrystalline graphite. *Shandong Chem. Ind.* **2015**, *44*, 151−152.
(15) Zhou, Y. Study on the treatment of high concentration fluorine-containing wastewater by chemical precipitation. *China Resour. Comprehens. Utili.* **2013**, *31* (02), 23−25.
(16) Millar, G. J.; Couperthwaite, S. J.; Wellner, D. B.; Macfarlane, D. C.; Dalzell, S. A. Removal of fluoride ions from solution by chelating resin with imino-diacetate functionality. *Journal of Water Process Engineering.* **2017**, *20*, 113−122.
(17) Zhou, Z.; Yan, W.; Gao, F.; Shi, M.; Shi, A. Adsorption and desorption of fluoride from zinc sulfate solution by D406 chelating resin. *Ion Exchange Adsorpt.* **2010**, *26* (02), 153−161.
(18) Shen, F.; Chen, X.; Gao, P.; Chen, G. Electrochemical removal of fluoride ions from industrial wastewater. *Chem. Eng. Sci.* **2003**, *58* (3−6), 987−993.
(19) Kang, H.; Zhang, D.; Chen, X.; Zhao, H.; Yang, D.; Li, Y.; Bao, M.; Wang, Z. Preparation of MOF/polypyrrole and flower-like MnO_2 electrodes by electrodeposition: High-performance materials for hybrid capacitive deionization defluorination. *Water Res.* **2023**, *229*, No. 119441.
(20) Bazrafshan, E.; Khoshnamvand, N.; Mahvi, A. H. Fluoride removal from aqueous environments by $ZnCl_2$-treated eucalyptus leaves as a natural adsorbent. *Fluoride* **2015**, *48* (4), 315−320.
(21) Kabay, N.; Arar, O.; Samatya, S.; Yuksel, U.; Yuksel, M. Separation of fluoride from aqueous solution by electrodialysis: effect of process parameters and other ionic species. *J. Hazard. Mater.* **2008**, *153* (1−2), 107−113.
(22) Lacson, C. F. Z.; Lu, M.; Huang, Y. Calcium-based seeded precipitation for simultaneous removal of fluoride and phosphate: Its optimization using BBD-RSM and defluoridation mechanism. *Journal of Water Process Engineering.* **2022**, *47*, No. 102658.
(23) Wang, X.; Shi, J.; Yan, S.; Lu, Z.; Gao, M. Study on the effect of PH value on the efficiency of fluoride removal by calcium chloride. *Consumer Guide* **2008**, *7*, 201.
(24) Liang, Y.; Che, Y.; Liu, X.; Li, N. *Data Handbook of Inorganic Thermodynamics*, 1st edition; Liang, Y.; Che, Y., Eds.; Academic Press: Shenyang, 1993; p 615.
(25) Yi, G.; Li, W.; Song, J.; Mei, B.; Zhou, Z.; Su, L. Structural, spectroscopic and thermal properties of hot-pressed Nd: $(Ca_{0.94}Gd_{0.06})F_{2.06}$ transparent ceramics. *Journal of the European Ceramic Society.* **2018**, *38* (9), 3240−3245.
(26) Ge, X.; Guo, Q.; Wang, Q.; Li, Tao; Liao, L. Mineralogical Characteristics and Luminescent Properties of Natural Fluorite with Three Different Colors. *Materials* **2022**, *15* (6), 1983.
(27) Mielczarski, E.; Mielczarski, J. A.; Cases, J. M.; Rai, B.; Pradip. Influence of solution conditions and mineral surface structure on the formation of oleate adsorption layers on fluorite. *Colloids and Surfaces A: Physicochemical and Engineering Aspects.* **2002**, *205* (1), 73−84.
(28) Zhang, Q.; Chen, L.; Wang, H.; Wang, X. Study on the performance and mechanism of fluoride removal by hydroxyl alumina with different aluminum sources. *Ind. Water Wastewater* **2015**, *46* (4), 23−28.

https://doi.org/10.1021/acsomega.4c06641
ACS Omega 2025, 10, 439−448